

## A POSTERIORI ERROR ANALYSIS OF AN AUGMENTED DUAL-MIXED METHOD IN LINEAR ELASTICITY WITH MIXED BOUNDARY CONDITIONS

TOMÁS P. BARRIOS, EDWIN M. BEHRENS, AND MARÍA GONZÁLEZ

**Abstract.** We consider an augmented mixed finite element method for the equations of plane linear elasticity with mixed boundary conditions. The method provides simultaneous approximations of the displacements, the stress tensor and the rotation. We develop an a posteriori error analysis based on the Ritz projection of the error and the use of an appropriate auxiliary function, and derive fully local reliable a posteriori error estimates that are locally efficient up to the elements that touch the Neumann boundary. We provide numerical experiments that illustrate the performance of the corresponding adaptive algorithm and support its use in practice.

**Key words.** a posteriori error estimates, mixed finite element, augmented formulation, stabilization, linear elasticity, Ritz projection.

### 1. Introduction

In this work, we consider the problem of plane linear elasticity with mixed boundary conditions. Typically, mixed finite element methods are used in linear elasticity to avoid the effects of locking while approximating additional unknowns of physical interest directly. It is well known that stable mixed finite elements for the linear elasticity problem involve many degrees of freedom. The application of stabilization techniques, such as augmented formulations, allows to use simpler finite element subspaces, including convenient equal-order interpolations that are generally unstable within the mixed approach.

In this framework, we consider the stabilized mixed finite element method presented in [7] for the problem of linear elasticity in the plane with homogeneous Dirichlet and non-homogeneous Neumann mixed boundary conditions. The approach in [7] relies on the mixed method of Hellinger and Reissner, that is enriched with suitable residual terms arising from the equilibrium equation, the constitutive law and the relation that defines the rotation in terms of the displacement. This approach leads to a well-posed, locking-free Galerkin scheme for any choice of finite element subspaces when homogeneous Dirichlet boundary conditions are prescribed. The method was successfully extended to the case of non-homogeneous Dirichlet boundary conditions in [8] (the three-dimensional version can be found in [9]).

In the case of mixed boundary conditions, which is the most usual in practice, the Neumann boundary condition is imposed weakly in [7], through the use of a Lagrange multiplier that can be interpreted as the trace of the displacement on the Neumann boundary. The resulting variational formulation has a saddle point structure. Hence, the analysis of the discrete scheme has to be done for any specific choice of finite element subspaces. In particular, it is possible to use Raviart-Thomas elements of the lowest order to approximate the stress tensor, continuous piecewise linear elements to approximate the displacement and piecewise constants

---

Received by the editors April 18, 2017 and accepted March 8, 2019.

2000 *Mathematics Subject Classification.* 65N15, 65N30, 65N50, 74B05, 74S05.

to approximate the rotation; the Lagrange multiplier on the Neumann boundary can be approximated by continuous piecewise linear elements on a suitable partition of that boundary, as we will see later. We should mention that an extension of the method proposed in [8, 9] to the case of mixed boundary conditions where the Neumann boundary condition is imposed in a strong sense has been analyzed recently in [11]. This extension leads to an augmented variational formulation with a coercive bilinear form and the corresponding Galerkin scheme is well-posed and free of locking for any choice of finite element subspaces.

Concerning the a posteriori error analysis of the augmented scheme presented in [7], an a posteriori error estimator of residual type was proposed in [1] in the case of pure homogeneous Dirichlet boundary conditions. That analysis was extended to the cases of pure non-homogeneous Dirichlet boundary conditions and mixed boundary conditions with non-homogeneous Neumann data in [2]. All these a posteriori error estimators are reliable and efficient, and involve the computation of at least eleven residuals per element. Moreover, they include normal and tangential jumps, and its extension to the three-dimensional case does not seem attractive. Recently, simpler a posteriori error estimators were introduced in [3] for the augmented schemes introduced in [7, 8, 9] in the case of boundary conditions of Dirichlet type. In the case of homogeneous boundary conditions, the new a posteriori error estimator introduced in [3] is reliable, locally efficient and only requires the computation of four residuals per element. Moreover, it is valid for two and three dimensional problems and for any finite element subspaces. When non-homogeneous boundary conditions are imposed, two new reliable a posteriori error estimators, one valid in 2D and 3D, and a second one that is only valid in 2D are proposed in [3]. The latter is locally efficient in the elements that do not touch the boundary and requires the computation of four residuals per element in the interior triangles, five residuals per element in the triangles with exactly one node on the boundary and six residuals per element in the triangles with a side on the boundary. Neither of these a posteriori error estimators require the computation of normal nor tangential jumps, which makes them easy to implement.

Our aim in this paper is to extend the analysis from [3] to the augmented dual-mixed method introduced in [7] in the case of mixed boundary conditions. With that purpose, we develop an a posteriori error analysis based on the Ritz projection of the error and obtain an a posteriori error estimator that is reliable and efficient, but that contains a non-local term. We then introduce an auxiliary function and derive fully local a posteriori error estimates that are reliable and locally efficient up to those elements that touch the Neumann boundary (see Theorem 5 below). As compared with the a posteriori error estimator introduced in [2] in the case of mixed boundary conditions, the a posteriori error estimates presented here are less expensive and easier to implement. Numerical experiments support the use of the new a posteriori error estimates in practice.

The rest of the paper is organized as follows. In Section 2, we recall the augmented variational formulation proposed in [7] for the linear elasticity problem in the plane with mixed boundary conditions and describe simple finite element subspaces that lead to a well-posed, locking-free Galerkin scheme. In Section 3, we develop the a posteriori error analysis and propose the new a posteriori error estimators. Finally, in Section 4 we provide several numerical experiments that support the use of the new a posteriori error estimates in practice.

We end this section with some notations to be used throughout the paper. Given a Hilbert space  $H$ , we denote by  $H^2$  (resp.,  $H^{2 \times 2}$ ) the space of vectors (resp., square

tensors) of order 2 with entries in  $H$ . Given  $\boldsymbol{\tau} := (\tau_{ij})$  and  $\boldsymbol{\zeta} := (\zeta_{ij}) \in \mathbb{R}^{2 \times 2}$ , we denote  $\boldsymbol{\tau}^\mathfrak{t} := (\tau_{ji})$ ,  $\text{tr}(\boldsymbol{\tau}) := \tau_{11} + \tau_{22}$  and  $\boldsymbol{\tau} : \boldsymbol{\zeta} := \sum_{i,j=1}^2 \tau_{ij} \zeta_{ij}$ . We also use the standard notations for Sobolev spaces and norms. Finally,  $C$  or  $c$  (with or without subscripts) denote generic constants, independent of the discretization parameters, that may take different values at different occurrences.

**2. The augmented mixed finite element method**

In this section we recall the augmented mixed finite element method introduced in [7] to solve the linear elasticity problem in the plane with mixed boundary conditions. Let  $\Omega \subset \mathbb{R}^2$  be a bounded and simply connected domain with a Lipschitz-continuous boundary  $\Gamma$ , and let  $\Gamma_D$  and  $\Gamma_N$  be two disjoint open subsets of  $\Gamma$  such that  $\Gamma = \bar{\Gamma}_D \cup \bar{\Gamma}_N$  and  $\Gamma_D$  has positive measure. We denote by  $\mathcal{C}$  the elasticity operator determined by Hooke’s law, that is,

$$\mathcal{C} \boldsymbol{\zeta} := \lambda \text{tr}(\boldsymbol{\zeta}) \mathbf{I} + 2 \mu \boldsymbol{\zeta}, \quad \forall \boldsymbol{\zeta} \in [L^2(\Omega)]^{2 \times 2},$$

where  $\lambda, \mu > 0$  are the Lamé parameters and  $\mathbf{I}$  is the identity matrix in  $\mathbb{R}^{2 \times 2}$ . It is easy to see that

$$\mathcal{C}^{-1} \boldsymbol{\zeta} := \frac{1}{2 \mu} \boldsymbol{\zeta} - \frac{\lambda}{4 \mu (\lambda + \mu)} \text{tr}(\boldsymbol{\zeta}) \mathbf{I}, \quad \forall \boldsymbol{\zeta} \in [L^2(\Omega)]^{2 \times 2}.$$

Now, assume we are given a volume force  $\mathbf{f} \in [L^2(\Omega)]^2$  and a traction  $\mathbf{g} \in [H^{-1/2}(\Gamma_N)]^2$ . We consider the problem: find the displacement  $\mathbf{u}$  and the stress tensor  $\boldsymbol{\sigma}$  such that

$$(1) \quad \begin{cases} -\text{div}(\boldsymbol{\sigma}) = \mathbf{f} & \text{in } \Omega, \\ \boldsymbol{\sigma} = \mathcal{C} \boldsymbol{\varepsilon}(\mathbf{u}) & \text{in } \Omega, \\ \mathbf{u} = \mathbf{0} & \text{on } \Gamma_D, \\ \boldsymbol{\sigma} \mathbf{n} = \mathbf{g} & \text{on } \Gamma_N, \end{cases}$$

where  $\boldsymbol{\varepsilon}(\mathbf{u}) := \frac{1}{2} (\nabla \mathbf{u} + (\nabla \mathbf{u})^\mathfrak{t})$  is the strain tensor of small deformations and  $\mathbf{n}$  is the unit outward normal to  $\Gamma$ . The approach in [7] provides simultaneous approximations of the displacement  $\mathbf{u}$ , the stress tensor  $\boldsymbol{\sigma}$ , the rotation  $\boldsymbol{\gamma} := \frac{1}{2} (\nabla \mathbf{u} - (\nabla \mathbf{u})^\mathfrak{t})$  and the Lagrange multiplier  $\boldsymbol{\xi} := -\mathbf{u}|_{\Gamma_N}$ .

Let  $\kappa_1, \kappa_2$  and  $\kappa_3$  be positive parameters, independent of  $\lambda$ , and define

$$H_{\Gamma_D}^1(\Omega) := \{v \in H^1(\Omega) : v = 0 \text{ on } \Gamma_D\},$$

$$H(\text{div}; \Omega) := \{\boldsymbol{\tau} \in [L^2(\Omega)]^{2 \times 2} : \text{div}(\boldsymbol{\tau}) \in [L^2(\Omega)]^2\}$$

and

$$[L^2(\Omega)]_{\text{skew}}^{2 \times 2} := \{\boldsymbol{\eta} \in [L^2(\Omega)]^{2 \times 2} : \boldsymbol{\eta} + \boldsymbol{\eta}^\mathfrak{t} = \mathbf{0}\}.$$

We recall that  $[H^{-1/2}(\Gamma_N)]^2$  is the dual of  $[H_{00}^{1/2}(\Gamma_N)]^2 := \{\mathbf{v}|_{\Gamma_N} : \mathbf{v} \in [H^1(\Omega)]^2, \mathbf{v} = \mathbf{0} \text{ on } \Gamma_D\}$  and denote by  $\langle \cdot, \cdot \rangle_{\Gamma_N}$  the associated duality pairing with respect to the  $[L^2(\Gamma_N)]^2$ -inner product. We define  $\mathbf{H} := H(\text{div}; \Omega) \times [H_{\Gamma_D}^1(\Omega)]^2 \times [L^2(\Omega)]_{\text{skew}}^{2 \times 2}$ ,  $\mathbf{Q} := [H_{00}^{1/2}(\Gamma_N)]^2$ , and consider the bilinear forms  $A : \mathbf{H} \times \mathbf{H} \rightarrow \mathbb{R}$  and  $B : \mathbf{H} \times \mathbf{Q} \rightarrow \mathbb{R}$ , and the linear functionals  $F : \mathbf{H} \rightarrow \mathbb{R}$  and  $G : \mathbf{Q} \rightarrow \mathbb{R}$  defined by

$$\begin{aligned}
& A((\boldsymbol{\sigma}, \mathbf{u}, \boldsymbol{\gamma}), (\boldsymbol{\tau}, \mathbf{v}, \boldsymbol{\eta})) \\
& := \int_{\Omega} \mathcal{C}^{-1} \boldsymbol{\sigma} : \boldsymbol{\tau} + \int_{\Omega} \mathbf{u} \cdot \mathbf{div}(\boldsymbol{\tau}) + \int_{\Omega} \boldsymbol{\tau} : \boldsymbol{\gamma} - \int_{\Omega} \mathbf{v} \cdot \mathbf{div}(\boldsymbol{\sigma}) \\
& \quad - \int_{\Omega} \boldsymbol{\sigma} : \boldsymbol{\eta} + \kappa_1 \int_{\Omega} (\boldsymbol{\varepsilon}(\mathbf{u}) - \mathcal{C}^{-1} \boldsymbol{\sigma}) : (\boldsymbol{\varepsilon}(\mathbf{v}) + \mathcal{C}^{-1} \boldsymbol{\tau}) \\
& \quad + \kappa_2 \int_{\Omega} \mathbf{div}(\boldsymbol{\sigma}) \cdot \mathbf{div}(\boldsymbol{\tau}) \\
& \quad + \kappa_3 \int_{\Omega} \left( \boldsymbol{\gamma} - \frac{1}{2}(\nabla \mathbf{u} - (\nabla \mathbf{u})^t) \right) : \left( \boldsymbol{\eta} + \frac{1}{2}(\nabla \mathbf{v} - (\nabla \mathbf{v})^t) \right), \\
& B((\boldsymbol{\tau}, \mathbf{v}, \boldsymbol{\eta}), \boldsymbol{\chi}) := \langle \boldsymbol{\tau} \mathbf{n}, \boldsymbol{\chi} \rangle_{\Gamma_N}, \\
& F(\boldsymbol{\tau}, \mathbf{v}, \boldsymbol{\eta}) := \int_{\Omega} \mathbf{f} \cdot (\mathbf{v} - \kappa_2 \mathbf{div}(\boldsymbol{\tau})), \\
& G(\boldsymbol{\chi}) := \langle \mathbf{g}, \boldsymbol{\chi} \rangle_{\Gamma_N},
\end{aligned}$$

for any  $(\boldsymbol{\sigma}, \mathbf{u}, \boldsymbol{\gamma}), (\boldsymbol{\tau}, \mathbf{v}, \boldsymbol{\eta}) \in \mathbf{H}$  and any  $\boldsymbol{\chi} \in \mathbf{Q}$ . We endow  $\mathbf{H}$  with the norm

$$\|(\boldsymbol{\tau}, \mathbf{v}, \boldsymbol{\eta})\|_{\mathbf{H}} := \left( \|\boldsymbol{\tau}\|_{H(\mathbf{div}; \Omega)}^2 + \|\mathbf{v}\|_{[H^1(\Omega)]^2}^2 + \|\boldsymbol{\eta}\|_{[L^2(\Omega)]^{2 \times 2}}^2 \right)^{1/2}, \quad \forall (\boldsymbol{\tau}, \mathbf{v}, \boldsymbol{\eta}) \in \mathbf{H}.$$

The augmented variational formulation proposed in [7] for problem (1) reads: find  $((\boldsymbol{\sigma}, \mathbf{u}, \boldsymbol{\gamma}), \boldsymbol{\xi}) \in \mathbf{H} \times \mathbf{Q}$  such that

$$(2) \quad \begin{cases} A((\boldsymbol{\sigma}, \mathbf{u}, \boldsymbol{\gamma}), (\boldsymbol{\tau}, \mathbf{v}, \boldsymbol{\eta})) + B((\boldsymbol{\tau}, \mathbf{v}, \boldsymbol{\eta}), \boldsymbol{\xi}) & = F(\boldsymbol{\tau}, \mathbf{v}, \boldsymbol{\eta}), \quad \forall (\boldsymbol{\tau}, \mathbf{v}, \boldsymbol{\eta}) \in \mathbf{H}, \\ B((\boldsymbol{\sigma}, \mathbf{u}, \boldsymbol{\gamma}), \boldsymbol{\chi}) & = G(\boldsymbol{\chi}), \quad \forall \boldsymbol{\chi} \in \mathbf{Q}. \end{cases}$$

Problem (2) exhibits a saddle-point structure; therefore, its analysis is based on the Babuška-Brezzi theory [4]. Hereafter, we assume that the stabilization parameters  $(\kappa_1, \kappa_2, \kappa_3)$  satisfy the assumptions of Theorem 3.3 in [7], namely,  $(\kappa_1, \kappa_2, \kappa_3)$  is independent of  $\lambda$ ,  $\kappa_1 \in (0, 2\mu)$ ,  $\kappa_2 > 0$  and  $\kappa_3 \in \left(0, \frac{k_D}{1 - k_D} \kappa_1\right)$ , where  $k_D \in (0, 1)$  is the constant of Korn's first inequality. We also recall that  $\mathbf{V} := \text{Ker}(B) = \{(\boldsymbol{\tau}, \mathbf{v}, \boldsymbol{\eta}) \in \mathbf{H} : \boldsymbol{\tau} \mathbf{n} = \mathbf{0} \text{ on } \Gamma_N\}$ . Then, the bilinear form  $A(\cdot, \cdot)$  is continuous in  $\mathbf{H}$  and  $\mathbf{V}$ -elliptic, that is, there exist positive constants  $M$  and  $\alpha$ , independent of  $\lambda$ , such that

$$|A((\boldsymbol{\sigma}, \mathbf{u}, \boldsymbol{\gamma}), (\boldsymbol{\tau}, \mathbf{v}, \boldsymbol{\eta}))| \leq M \|(\boldsymbol{\sigma}, \mathbf{u}, \boldsymbol{\gamma})\|_{\mathbf{H}} \|(\boldsymbol{\tau}, \mathbf{v}, \boldsymbol{\eta})\|_{\mathbf{H}}, \quad \forall (\boldsymbol{\sigma}, \mathbf{u}, \boldsymbol{\gamma}), (\boldsymbol{\tau}, \mathbf{v}, \boldsymbol{\eta}) \in \mathbf{H},$$

and

$$A((\boldsymbol{\tau}, \mathbf{v}, \boldsymbol{\eta}), (\boldsymbol{\tau}, \mathbf{v}, \boldsymbol{\eta})) \geq \alpha \|(\boldsymbol{\tau}, \mathbf{v}, \boldsymbol{\eta})\|_{\mathbf{H}}^2, \quad \forall (\boldsymbol{\tau}, \mathbf{v}, \boldsymbol{\eta}) \in \mathbf{V}.$$

Moreover, the bilinear form  $B(\cdot, \cdot)$  satisfies the following inf-sup condition:

$$\sup_{\substack{\boldsymbol{\tau} \in \tilde{H}_0 \\ \boldsymbol{\tau} \neq \mathbf{0}}} \frac{B((\boldsymbol{\tau}, \mathbf{v}, \boldsymbol{\eta}), \boldsymbol{\chi})}{\|\boldsymbol{\tau}\|_{H(\mathbf{div}; \Omega)}} \geq \beta \|\boldsymbol{\chi}\|_{\mathbf{Q}}, \quad \forall \boldsymbol{\chi} \in \mathbf{Q},$$

where  $\beta$  is a positive constant, independent of  $\lambda$ , and  $\tilde{H}_0 = \{\boldsymbol{\tau} \in H(\mathbf{div}; \Omega) : \boldsymbol{\tau} = \boldsymbol{\tau}^t, \mathbf{div}(\boldsymbol{\tau}) = \mathbf{0} \text{ in } \Omega\}$ . As a consequence, the augmented variational formulation (2) has a unique solution  $((\boldsymbol{\sigma}, \mathbf{u}, \boldsymbol{\gamma}), \boldsymbol{\xi}) \in \mathbf{H} \times \mathbf{Q}$  and there exists a positive constant  $C$ , independent of  $\lambda$ , such that

$$\|((\boldsymbol{\sigma}, \mathbf{u}, \boldsymbol{\gamma}), \boldsymbol{\xi})\|_{\mathbf{H} \times \mathbf{Q}} \leq C \left( \|\mathbf{f}\|_{[L^2(\Omega)]^2} + \|\mathbf{g}\|_{[H^{-1/2}(\Gamma_N)]^2} \right).$$



where  $\langle \cdot, \cdot \rangle_{\Gamma_N}$  denote the duality pairing between  $H^{-1/2}(\Gamma_N)$  and  $H_{00}^{1/2}(\Gamma_N)$  with respect to  $L^2(\Gamma_N)$ -inner product.

*Proof.* First, we remark that if  $\gamma_h$  is of bounded variation, then  $\gamma_{\tilde{h}}$  is of bounded variation as well. Let us assume, for simplicity, that  $n$  is even. Then,  $m = \frac{n}{2}$  and the dimension of  $Q_{\tilde{h}}$  is  $m - 1$ . For each  $\tilde{e}_i \in \gamma_{\tilde{h}}$ , there exist two elements,  $l_i, r_i \in \gamma_h$ , such that  $\tilde{e}_i = l_i \cup r_i$ . We tagged  $l_i$  and  $r_i$  as left and right in the numbering direction of  $\gamma_{\tilde{h}}$ , so that  $r_i$  is adjacent to  $l_{i+1}$ . Then, using that  $\gamma_{\tilde{h}}$  is of bounded variation, it follows that

$$0 < C_1 \leq c_i := \frac{|r_i|}{|\tilde{e}_i|} \leq C_2 < 1, \quad \forall i = 1, \dots, m,$$

and

$$0 < C_3 \leq \frac{|\tilde{e}_i|}{|\tilde{e}_{i+1}|} \leq C_4 \quad \forall i = 1, \dots, m - 1.$$

Now, for each  $i = 1, \dots, m - 1$ , we introduce the constant functions

$$\chi_i := \begin{cases} c_i^{-1} & \text{in } r_i \\ (1 - c_{i+1})^{-1} & \text{in } l_{i+1} \\ 0 & \text{otherwise} \end{cases}$$

and the discrete space  $\Phi_{\tilde{h}}^0 := \text{span}\{\chi_1, \chi_2, \dots, \chi_{m-1}\} \subset \Phi_h$ . It is not difficult to see that the constant functions  $\chi_i$  are mutually orthogonal, so that the dimension of  $\Phi_{\tilde{h}}^0$  is  $m - 1$ , that is, is equal to dimension of  $Q_{\tilde{h}}$ . Then, the proof follows as in Lemma 5.2 in [10].  $\square$

**Remark.** To ensure that  $\gamma_h$  is of bounded variation, it is enough that the triangulation  $\mathcal{T}_h$  is quasiuniform in a neighborhood of  $\Gamma_N$ .  $\square$

From the previous Lemma, there exists  $C > 0$ , independent of  $h$  and  $\tilde{h}$ , such that the following discrete inf-sup condition is satisfied:

$$\sup_{\boldsymbol{\rho}_h \in [\Phi_h]^2 \setminus \{\mathbf{0}\}} \frac{\langle \boldsymbol{\rho}_h, \boldsymbol{\chi}_{\tilde{h}} \rangle_{\Gamma_N}}{\|\boldsymbol{\rho}_h\|_{[H^{-1/2}(\Gamma_N)]^2}} \geq C \|\boldsymbol{\chi}_{\tilde{h}}\|_{[H_{00}^{1/2}(\Gamma_N)]^2}, \quad \forall \boldsymbol{\chi}_{\tilde{h}} \in \mathbf{Q}_{\tilde{h}}.$$

In this case, the well-posedness and stability of the Galerkin scheme (3) holds if we assume that the family of triangulations  $\{\mathcal{T}_h\}_{h>0}$  is uniformly regular on  $\Gamma_N$  (in order to apply Lemma 4.6 in [7]).

In the following Theorem, we recall the rate of convergence of the Galerkin scheme (3) for this particular choice of finite element subspaces.

**Theorem 2.** *Let  $((\boldsymbol{\sigma}, \mathbf{u}, \boldsymbol{\gamma}), \boldsymbol{\xi}) \in \mathbf{H} \times \mathbf{Q}$  and  $((\boldsymbol{\sigma}_h, \mathbf{u}_h, \boldsymbol{\gamma}_h), \boldsymbol{\xi}_{\tilde{h}}) \in \mathbf{H}_h \times \mathbf{Q}_{\tilde{h}}$  be the unique solutions to problems (2) and (3), respectively. Assume that  $\boldsymbol{\sigma} \in [H^r(\Omega)]^{2 \times 2}$ ,  $\text{div}(\boldsymbol{\sigma}) \in [H^r(\Omega)]^2$ ,  $\mathbf{u} \in [H^{r+1}(\Omega)]^2$ ,  $\boldsymbol{\gamma} \in [H^r(\Omega)]^{2 \times 2}$  and  $\boldsymbol{\xi} \in [H_{00}^{r+1/2}(\Gamma_N)]^2$ , for some  $r \in (0, 1]$ . Then, there exists  $C > 0$ , independent of  $\lambda, h$  and  $\tilde{h}$ , such that there holds*

$$\begin{aligned} & \|((\boldsymbol{\sigma}, \mathbf{u}, \boldsymbol{\gamma}), \boldsymbol{\xi}) - ((\boldsymbol{\sigma}_h, \mathbf{u}_h, \boldsymbol{\gamma}_h), \boldsymbol{\xi}_{\tilde{h}})\|_{\mathbf{H} \times \mathbf{Q}} \leq C \tilde{h}^r \|\boldsymbol{\xi}\|_{[H_{00}^{r+1/2}(\Gamma_N)]^2} \\ & + C h^r \left( \|\boldsymbol{\sigma}\|_{[H^r(\Omega)]^{2 \times 2}} + \|\text{div}(\boldsymbol{\sigma})\|_{[H^r(\Omega)]^2} + \|\mathbf{u}\|_{[H^{r+1}(\Omega)]^2} + \|\boldsymbol{\gamma}\|_{[H^r(\Omega)]^{2 \times 2}} \right). \end{aligned}$$

*Proof.* See Theorem 4.10 in [7] and take into account the definition of  $\gamma_{\tilde{h}}$ .  $\square$

### 3. A posteriori error analysis

In this section, we follow [3] and develop an a posteriori error analysis for the discrete scheme (3) using an appropriate Ritz projection of the error. Given a triangle  $T \in \mathcal{T}_h$ , we denote by  $E(T)$  the set of its edges, and denote by  $E_h(\Gamma_N)$  the set of all the edges in  $\mathcal{T}_h$  contained in  $\Gamma_N$ . Then, we assume that each side  $e_i \in E_h(\Gamma_N)$ ,  $i \in \{1, \dots, n\}$ , is contained in a side  $\tilde{e}_j$ , for some  $j \in \{1, \dots, m\}$ ; in this case, we denote by  $\tilde{h}_{e_i} = |\tilde{e}_j|$ .

Let  $((\boldsymbol{\sigma}, \mathbf{u}, \boldsymbol{\gamma}), \boldsymbol{\xi})$  be the unique solution to problem (2) and assume that the Galerkin scheme (3) has a unique solution,  $((\boldsymbol{\sigma}_h, \mathbf{u}_h, \boldsymbol{\gamma}_h), \boldsymbol{\xi}_{\tilde{h}})$ , that depends continuously on the data. We define the Ritz projection of the error with respect to the inner product of  $\mathbf{H}$ ,

$$\langle (\boldsymbol{\sigma}, \mathbf{u}, \boldsymbol{\gamma}), (\boldsymbol{\tau}, \mathbf{v}, \boldsymbol{\eta}) \rangle_{\mathbf{H}} := (\boldsymbol{\sigma}, \boldsymbol{\tau})_{H(\operatorname{div}; \Omega)} + (\mathbf{u}, \mathbf{v})_{[H^1(\Omega)]^2} + (\boldsymbol{\gamma}, \boldsymbol{\eta})_{[L^2(\Omega)]^{2 \times 2}},$$

as the unique element  $(\bar{\boldsymbol{\sigma}}, \bar{\mathbf{u}}, \bar{\boldsymbol{\gamma}}) \in \mathbf{H}$  such that for all  $(\boldsymbol{\tau}, \mathbf{v}, \boldsymbol{\eta}) \in \mathbf{H}$ ,

$$(4) \quad \langle (\bar{\boldsymbol{\sigma}}, \bar{\mathbf{u}}, \bar{\boldsymbol{\gamma}}), (\boldsymbol{\tau}, \mathbf{v}, \boldsymbol{\eta}) \rangle_{\mathbf{H}} = A((\boldsymbol{\sigma} - \boldsymbol{\sigma}_h, \mathbf{u} - \mathbf{u}_h, \boldsymbol{\gamma} - \boldsymbol{\gamma}_h), (\boldsymbol{\tau}, \mathbf{v}, \boldsymbol{\eta})) + B((\boldsymbol{\tau}, \mathbf{v}, \boldsymbol{\eta}), \boldsymbol{\xi} - \boldsymbol{\xi}_{\tilde{h}}).$$

We remark that the existence and uniqueness of  $(\bar{\boldsymbol{\sigma}}, \bar{\mathbf{u}}, \bar{\boldsymbol{\gamma}}) \in \mathbf{H}$  is guaranteed by the Lax-Milgram Lemma.

Using the continuous dependence of the solution on the data, we are able to bound the error in terms of its Ritz projection and the residual in the Neumann boundary condition, that is,

$$(5) \quad \begin{aligned} & \|((\boldsymbol{\sigma} - \boldsymbol{\sigma}_h, \mathbf{u} - \mathbf{u}_h, \boldsymbol{\gamma} - \boldsymbol{\gamma}_h), \boldsymbol{\xi} - \boldsymbol{\xi}_{\tilde{h}})\|_{\mathbf{H} \times \mathbf{Q}} \leq \\ & \leq C \left( \|(\bar{\boldsymbol{\sigma}}, \bar{\mathbf{u}}, \bar{\boldsymbol{\gamma}})\|_{\mathbf{H}} + \|\mathbf{g} - \boldsymbol{\sigma}_h \mathbf{n}\|_{[H^{-1/2}(\Gamma_N)]^2} \right). \end{aligned}$$

Assume that  $\mathbf{g} \in [L^2(\Gamma_N)]^2$ . Then, applying Theorem 2 in [5] (see also [2, (2.16)]), the residual in the Neumann boundary condition can be bounded in terms of a  $L^2$ -norm:

$$(6) \quad \|\mathbf{g} - \boldsymbol{\sigma}_h \mathbf{n}\|_{[H^{-1/2}(\Gamma_N)]^2}^2 \leq C \log(1 + \kappa) \sum_{e \in E_h(\Gamma_N)} \tilde{h}_e \|\mathbf{g} - \boldsymbol{\sigma}_h \mathbf{n}\|_{[L^2(e)]^2}^2,$$

where  $\kappa := \max \left\{ \frac{|e_i|}{|e_j|} : e_i \text{ is a neighbor of } e_j \right\}$ . Then, according to (5), to obtain reliable a posteriori error estimates for the discrete scheme (3), it is enough to bound from above the Ritz projection of the error. In the next lemma we obtain an upper bound for  $\|(\bar{\boldsymbol{\sigma}}, \bar{\mathbf{u}}, \bar{\boldsymbol{\gamma}})\|_{\mathbf{H}}$  in terms of residuals.

**Lemma 3.** *There exists a constant  $C > 0$ , independent of  $h$ ,  $\tilde{h}$  and  $\lambda$ , such that*

$$(7) \quad \begin{aligned} \|(\bar{\boldsymbol{\sigma}}, \bar{\mathbf{u}}, \bar{\boldsymbol{\gamma}})\|_{\mathbf{H}} & \leq C \left( \|\mathbf{f} + \operatorname{div}(\boldsymbol{\sigma}_h)\|_{[L^2(\Omega)]^2} + \|\boldsymbol{\sigma}_h - \boldsymbol{\sigma}_h^{\ddagger}\|_{[L^2(\Omega)]^{2 \times 2}} \right. \\ & \quad + \|\mathbf{u}_h + \boldsymbol{\xi}_{\tilde{h}}\|_{[H_{00}^{1/2}(\Gamma_N)]^2} + \|\boldsymbol{\varepsilon}(\mathbf{u}_h) - \mathcal{C}^{-1} \boldsymbol{\sigma}_h\|_{[L^2(\Omega)]^{2 \times 2}} \\ & \quad \left. + \|\boldsymbol{\gamma}_h - \frac{1}{2}(\nabla \mathbf{u}_h - (\nabla \mathbf{u}_h)^{\ddagger})\|_{[L^2(\Omega)]^{2 \times 2}} \right). \end{aligned}$$

*Proof.* We first use that  $((\boldsymbol{\sigma}, \mathbf{u}, \boldsymbol{\gamma}), \boldsymbol{\xi})$  is the unique solution to problem (2) to write  $\langle (\bar{\boldsymbol{\sigma}}, \bar{\mathbf{u}}, \bar{\boldsymbol{\gamma}}), (\boldsymbol{\tau}, \mathbf{v}, \boldsymbol{\eta}) \rangle_{\mathbf{H}} = F(\boldsymbol{\tau}, \mathbf{v}, \boldsymbol{\eta}) - A((\boldsymbol{\sigma}_h, \mathbf{u}_h, \boldsymbol{\gamma}_h), (\boldsymbol{\tau}, \mathbf{v}, \boldsymbol{\eta})) - B((\boldsymbol{\tau}, \mathbf{v}, \boldsymbol{\eta}), \boldsymbol{\xi}_{\tilde{h}})$ , for all  $(\boldsymbol{\tau}, \mathbf{v}, \boldsymbol{\eta}) \in \mathbf{H}$ . Equivalently,

$$\begin{aligned} (\bar{\boldsymbol{\sigma}}, \boldsymbol{\tau})_{H(\operatorname{div}; \Omega)} & = F_1(\boldsymbol{\tau}), & \forall \boldsymbol{\tau} \in H(\operatorname{div}; \Omega), \\ (\bar{\mathbf{u}}, \mathbf{v})_{[H^1(\Omega)]^2} & = F_2(\mathbf{v}), & \forall \mathbf{v} \in [H_{\Gamma_D}^1(\Omega)]^2, \\ (\bar{\boldsymbol{\gamma}}, \boldsymbol{\eta})_{[L^2(\Omega)]^{2 \times 2}} & = F_3(\boldsymbol{\eta}), & \forall \boldsymbol{\eta} \in [L^2(\Omega)]_{\text{skew}}^{2 \times 2}, \end{aligned}$$

where  $F_1 : H(\mathbf{div}; \Omega) \rightarrow \mathbb{R}$ ,  $F_2 : [H_{\Gamma_D}^1(\Omega)]^2 \rightarrow \mathbb{R}$  and  $F_3 : [L^2(\Omega)]_{\text{skew}}^{2 \times 2} \rightarrow \mathbb{R}$  are the bounded linear functionals defined by

$$\begin{aligned} F_1(\boldsymbol{\tau}) &:= -\kappa_2 \int_{\Omega} (\mathbf{f} + \mathbf{div}(\boldsymbol{\sigma}_h)) \cdot \mathbf{div}(\boldsymbol{\tau}) - \int_{\Omega} (\mathcal{C}^{-1} \boldsymbol{\sigma}_h - \nabla \mathbf{u}_h + \boldsymbol{\gamma}_h) : \boldsymbol{\tau} \\ &\quad - \kappa_1 \int_{\Omega} \mathcal{C}^{-1} (\boldsymbol{\varepsilon}(\mathbf{u}_h) - \mathcal{C}^{-1} \boldsymbol{\sigma}_h) : \boldsymbol{\tau} - \langle \boldsymbol{\tau} \mathbf{n}, \boldsymbol{\xi}_{\tilde{h}} + \mathbf{u}_h \rangle_{\Gamma_N}, \\ F_2(\mathbf{v}) &:= \int_{\Omega} (\mathbf{f} + \mathbf{div}(\boldsymbol{\sigma}_h)) \cdot \mathbf{v} - \kappa_1 \int_{\Omega} (\boldsymbol{\varepsilon}(\mathbf{u}_h) - \frac{1}{2} \mathcal{C}^{-1} (\boldsymbol{\sigma}_h + \boldsymbol{\sigma}_h^{\dagger})) : \nabla \mathbf{v} \\ &\quad - \kappa_3 \int_{\Omega} (\boldsymbol{\gamma}_h - \frac{1}{2} (\nabla \mathbf{u}_h - (\nabla \mathbf{u}_h)^{\dagger})) : \nabla \mathbf{v}, \\ F_3(\boldsymbol{\eta}) &:= \int_{\Omega} \frac{1}{2} (\boldsymbol{\sigma}_h - \boldsymbol{\sigma}_h^{\dagger}) : \boldsymbol{\eta} - \kappa_3 \int_{\Omega} (\boldsymbol{\gamma}_h - \frac{1}{2} (\nabla \mathbf{u}_h - (\nabla \mathbf{u}_h)^{\dagger})) : \boldsymbol{\eta}. \end{aligned}$$

Then, the result follows using the Cauchy-Schwarz inequality, the triangle inequality, the continuity of  $\mathcal{C}^{-1}$  and the definition of the  $\mathbf{H}$ -norm.  $\square$

Motivated by the previous results, we define the a posteriori error estimate

$$\eta := \left( \sum_{T \in \mathcal{T}_h} \eta_T^2 + \|\mathbf{u}_h + \boldsymbol{\xi}_{\tilde{h}}\|_{[H_{00}^{1/2}(\Gamma_N)]^2}^2 \right)^{1/2},$$

where

$$\begin{aligned} \eta_T^2 &:= \|\mathbf{f} + \mathbf{div}(\boldsymbol{\sigma}_h)\|_{[L^2(T)]^2}^2 + \|\boldsymbol{\sigma}_h - \boldsymbol{\sigma}_h^{\dagger}\|_{[L^2(T)]^{2 \times 2}}^2 \\ &\quad + \log(1 + \kappa) \sum_{e \in E(T) \cap E_h(\Gamma_N)} \tilde{h}_e \|\mathbf{g} - \boldsymbol{\sigma}_h \mathbf{n}\|_{[L^2(e)]^2}^2 \\ &\quad + \|\boldsymbol{\varepsilon}(\mathbf{u}_h) - \mathcal{C}^{-1} \boldsymbol{\sigma}_h\|_{[L^2(T)]^{2 \times 2}}^2 + \left\| \boldsymbol{\gamma}_h - \frac{1}{2} (\nabla \mathbf{u}_h - (\nabla \mathbf{u}_h)^{\dagger}) \right\|_{[L^2(T)]^{2 \times 2}}^2. \end{aligned}$$

We recall that any  $T \in \mathcal{T}_h$  has at most one of its sides on  $\Gamma_N$ . In the next theorem we establish that the a posteriori error estimator  $\eta$  is reliable and efficient.

**Theorem 4.** *Assume that  $\mathbf{g} \in [L^2(\Gamma_N)]^2$ . Then, there exist positive constants,  $C_{\text{eff}}$  and  $C_{\text{rel}}$ , independent of  $h$ ,  $\tilde{h}$  and  $\lambda$ , such that*

$$C_{\text{eff}} \eta \leq \|((\boldsymbol{\sigma} - \boldsymbol{\sigma}_h, \mathbf{u} - \mathbf{u}_h, \boldsymbol{\gamma} - \boldsymbol{\gamma}_h), \boldsymbol{\xi} - \boldsymbol{\xi}_{\tilde{h}})\|_{\mathbf{H} \times \mathbf{Q}} \leq C_{\text{rel}} \eta.$$

*Proof.* The reliability of  $\eta$  (second inequality above) follows from its definition and inequalities (5)–(7). To prove that  $\eta$  is efficient, we recall that  $\boldsymbol{\xi} = -\mathbf{u}$  on  $\Gamma_N$  and use the triangle inequality and a trace theorem to get

$$\begin{aligned} \|\mathbf{u}_h + \boldsymbol{\xi}_{\tilde{h}}\|_{[H_{00}^{1/2}(\Gamma_N)]^2} &\leq \|\mathbf{u}_h - \mathbf{u}\|_{[H_{00}^{1/2}(\Gamma_N)]^2} + \|\boldsymbol{\xi}_{\tilde{h}} - \boldsymbol{\xi}\|_{[H_{00}^{1/2}(\Gamma_N)]^2} \\ &\leq C \|\mathbf{u}_h - \mathbf{u}\|_{[H^1(\Omega)]^2} + \|\boldsymbol{\xi}_{\tilde{h}} - \boldsymbol{\xi}\|_{[H_{00}^{1/2}(\Gamma_N)]^2}. \end{aligned}$$

On the other hand, from the proof of Lemma 6.5 in [6] (see also [2]), we deduce that

$$\begin{aligned} (8) \quad &\sum_{e \in E(T) \cap E_h(\Gamma_N)} \tilde{h}_e \|\mathbf{g} - \boldsymbol{\sigma}_h \mathbf{n}\|_{[L^2(e)]^2}^2 \leq \\ &\leq C \sum_{e \in E(T) \cap E_h(\Gamma_N)} \left( h_T^2 \|\mathbf{div}(\boldsymbol{\sigma} - \boldsymbol{\sigma}_h)\|_{[L^2(T)]^2}^2 + \|\boldsymbol{\sigma} - \boldsymbol{\sigma}_h\|_{[L^2(T)]^2}^2 \right) \end{aligned}$$

The result follows proceeding with the remaining terms as in [1].  $\square$

Since the a posteriori error estimate  $\eta$  is not fully local, it cannot be used in an adaptive algorithm. A first attempt to define a reliable and fully local a posteriori error estimator can be achieved by using an interpolation argument. Indeed, it suffices to remark that the space  $[H_{00}^{1/2}(\Gamma_N)]^2$  is the interpolation space of index 1/2 between  $[H_0^1(\Gamma_N)]^2$  and  $[L^2(\Gamma_N)]^2$ . Then, if  $\mathbf{g} \in [L^2(\Gamma_N)]^2$ , there exists a constant  $C_{\text{rel}} > 0$ , independent of  $h$ ,  $\tilde{h}$  and  $\lambda$ , such that

$$\|((\boldsymbol{\sigma} - \boldsymbol{\sigma}_h, \mathbf{u} - \mathbf{u}_h, \boldsymbol{\gamma} - \boldsymbol{\gamma}_h), \boldsymbol{\xi} - \boldsymbol{\xi}_{\tilde{h}})\|_{\mathbf{H} \times \mathbf{Q}} \leq C_{\text{rel}} \hat{\eta}$$

where

$$\hat{\eta} := \left( \sum_{T \in \mathcal{T}_h} \hat{\eta}_T^2 \right)^{1/2}, \quad \text{with} \quad \hat{\eta}_T^2 := \eta_T^2 + \sum_{e \in E(T) \cap E_h(\Gamma_N)} \|\mathbf{u}_h + \boldsymbol{\xi}_{\tilde{h}}\|_{[H^1(e)]^2}^2.$$

An alternative approach, based on the introduction of an auxiliary function (see [5]), allows us to derive a fully local, reliable and *quasi-efficient* a posteriori error estimate. Indeed, let  $\bar{\mathbf{u}}_h$  be the unique continuous piecewise linear function defined in  $\bar{\Omega}$  such that  $\bar{\mathbf{u}}_h(\mathbf{x}) = \mathbf{u}_h(\mathbf{x})$  for all node  $\mathbf{x}$  of  $\mathcal{T}_h$  in  $\Omega \cup \Gamma_D$  and  $\bar{\mathbf{u}}_h(\mathbf{x}) = -\boldsymbol{\xi}_{\tilde{h}}(\mathbf{x})$  for all node  $\mathbf{x}$  of  $\mathcal{T}_h$  on  $\Gamma_N$ . We remark that  $\bar{\mathbf{u}}_h$  is defined so that  $\bar{\mathbf{u}}_h + \boldsymbol{\xi}_{\tilde{h}}$  vanishes at the nodes of  $\mathcal{T}_h$  on  $\Gamma_N$ .

**Lemma 5.** *There exists a constant  $C > 0$ , independent of  $h$ ,  $\tilde{h}$  and  $\lambda$ , such that*

$$\begin{aligned} \|(\bar{\boldsymbol{\sigma}}, \bar{\mathbf{u}}, \bar{\boldsymbol{\gamma}})\|_{\mathbf{H}} &\leq C \left( \|\mathbf{f} + \mathbf{div}(\boldsymbol{\sigma}_h)\|_{[L^2(\Omega)]^2} + \|\boldsymbol{\sigma}_h - \boldsymbol{\sigma}_h^\dagger\|_{[L^2(\Omega)]^{2 \times 2}} \right. \\ &\quad + \|\bar{\mathbf{u}}_h + \boldsymbol{\xi}_{\tilde{h}}\|_{[H_{00}^{1/2}(\Gamma_N)]^2} + \|\boldsymbol{\varepsilon}(\mathbf{u}_h) - \mathcal{C}^{-1}\boldsymbol{\sigma}_h\|_{[L^2(\Omega)]^{2 \times 2}} \\ &\quad \left. + \|\boldsymbol{\gamma}_h - \frac{1}{2}(\nabla \mathbf{u}_h - (\nabla \mathbf{u}_h)^\dagger)\|_{[L^2(\Omega)]^{2 \times 2}} + \|\mathbf{u}_h - \bar{\mathbf{u}}_h\|_{[H^1(\Omega)]^2} \right). \end{aligned}$$

*Proof.* The proof is analogous to that of Lemma 3, but with

$$\begin{aligned} F_1(\boldsymbol{\tau}) &:= -\kappa_2 \int_{\Omega} (\mathbf{f} + \mathbf{div}(\boldsymbol{\sigma}_h)) \cdot \mathbf{div}(\boldsymbol{\tau}) + \int_{\Omega} (\mathbf{u}_h - \bar{\mathbf{u}}_h) \cdot \mathbf{div}(\boldsymbol{\tau}) \\ &\quad - \int_{\Omega} (\mathcal{C}^{-1}\boldsymbol{\sigma}_h - \nabla \bar{\mathbf{u}}_h + \boldsymbol{\gamma}_h) : \boldsymbol{\tau} \\ &\quad - \kappa_1 \int_{\Omega} \mathcal{C}^{-1}(\boldsymbol{\varepsilon}(\mathbf{u}_h) - \mathcal{C}^{-1}\boldsymbol{\sigma}_h) : \boldsymbol{\tau} - \langle \boldsymbol{\tau} \mathbf{n}, \boldsymbol{\xi}_{\tilde{h}} + \bar{\mathbf{u}}_h \rangle_{\Gamma_N} \quad \forall \boldsymbol{\tau} \in H(\mathbf{div}; \Omega). \end{aligned}$$

We remark that we bound

$$\begin{aligned} \|\mathcal{C}^{-1}\boldsymbol{\sigma}_h - \nabla \bar{\mathbf{u}}_h + \boldsymbol{\gamma}_h\|_{[L^2(\Omega)]^{2 \times 2}} &\leq \|\boldsymbol{\varepsilon}(\mathbf{u}_h) - \mathcal{C}^{-1}\boldsymbol{\sigma}_h\|_{[L^2(\Omega)]^{2 \times 2}} \\ &\quad + \|\boldsymbol{\gamma}_h - \frac{1}{2}(\nabla \mathbf{u}_h - (\nabla \mathbf{u}_h)^\dagger)\|_{[L^2(\Omega)]^{2 \times 2}} + \|\nabla(\mathbf{u}_h - \bar{\mathbf{u}}_h)\|_{[L^2(\Omega)]^{2 \times 2}}. \end{aligned}$$

□

Now, since  $\bar{\mathbf{u}}_h + \boldsymbol{\xi}_{\tilde{h}}$  vanishes on the nodes of  $\mathcal{T}_h$  on  $\Gamma_N$ , by virtue of Theorem 1 in [5], if  $|\Gamma_D| \geq |\tilde{e}_1| + |\tilde{e}_m|$ , we have that

$$(9) \quad \|\bar{\mathbf{u}}_h + \boldsymbol{\xi}_{\tilde{h}}\|_{[H_{00}^{1/2}(\Gamma_N)]^2} \leq C \log(1 + \kappa) \sum_{e \in E_h(\Gamma_N)} h_e \left\| \frac{d}{dt_T} (\bar{\mathbf{u}}_h + \boldsymbol{\xi}_{\tilde{h}}) \right\|_{[L^2(e)]^2}^2,$$

where  $\mathbf{t}_T$  denotes the unit tangential vector along  $e$ . This result motivates the definition of the fully local a posteriori error estimate  $\bar{\eta} := \left( \sum_{T \in \mathcal{T}_h} \bar{\eta}_T^2 \right)^{1/2}$ , where

$$\begin{aligned} \bar{\eta}_T^2 &:= \|\mathbf{f} + \mathbf{div}(\boldsymbol{\sigma}_h)\|_{[L^2(T)]^2}^2 + \|\boldsymbol{\sigma}_h - \boldsymbol{\sigma}_h^\ddagger\|_{[L^2(T)]^{2 \times 2}}^2 + \|\mathbf{u}_h - \bar{\mathbf{u}}_h\|_{[H^1(T)]^2}^2 \\ &+ \|\boldsymbol{\varepsilon}(\mathbf{u}_h) - \mathcal{C}^{-1} \boldsymbol{\sigma}_h\|_{[L^2(T)]^{2 \times 2}}^2 + \|\boldsymbol{\gamma}_h - \frac{1}{2} (\nabla \mathbf{u}_h - (\nabla \mathbf{u}_h)^\mathbf{t})\|_{[L^2(T)]^{2 \times 2}}^2 \\ &+ \log(1 + \kappa) \sum_{e \in E(T) \cap E_h(\Gamma_N)} \left( \tilde{h}_e \|\mathbf{g} - \boldsymbol{\sigma}_h \mathbf{n}\|_{[L^2(e)]^2}^2 \right. \\ &\left. + h_e \left\| \frac{d}{dt} (\bar{\mathbf{u}}_h + \boldsymbol{\xi}_{\tilde{h}}) \right\|_{[L^2(e)]^2}^2 \right). \end{aligned}$$

**Theorem 6.** *Assume that  $\mathbf{g} \in [L^2(\Gamma_N)]^2$  and  $|\Gamma_D| \geq |\tilde{e}_1| + |\tilde{e}_m|$ . Then there exists positive constants,  $C_{\text{eff}}$  and  $C_{\text{rel}}$ , independent of  $h$ ,  $\tilde{h}$  and  $\lambda$ , such that*

$$\|((\boldsymbol{\sigma} - \boldsymbol{\sigma}_h, \mathbf{u} - \mathbf{u}_h, \boldsymbol{\gamma} - \boldsymbol{\gamma}_h), \boldsymbol{\xi} - \boldsymbol{\xi}_{\tilde{h}})\|_{\mathbf{H} \times \mathbf{Q}} \leq C_{\text{rel}} \bar{\eta},$$

and

$$\begin{aligned} C_{\text{eff}} \bar{\eta} &\leq \|((\boldsymbol{\sigma} - \boldsymbol{\sigma}_h, \mathbf{u} - \mathbf{u}_h, \boldsymbol{\gamma} - \boldsymbol{\gamma}_h), \boldsymbol{\xi} - \boldsymbol{\xi}_{\tilde{h}})\|_{\mathbf{H} \times \mathbf{Q}} \\ &+ \left( \sum_{\substack{T \in \mathcal{T}_h \\ \partial T \cap \bar{\Gamma}_N \neq \emptyset}} \|\mathbf{u} - \bar{\mathbf{u}}_h\|_{[H^1(T)]^2}^2 \right)^{1/2}. \end{aligned}$$

*Proof.* The reliability estimate follows from (5), (6), Lemma 5, (9) and the definition of  $\bar{\eta}$ . To prove the second inequality, we proceed similarly as in Subsection 2.3.2 in [2] and obtain that

$$\sum_{e \in E_h(\Gamma_N)} h_e \left\| \frac{d}{dt} (\bar{\mathbf{u}}_h + \boldsymbol{\xi}_{\tilde{h}}) \right\|_{[L^2(e)]^2}^2 \leq C \left( \|\mathbf{u}_h - \mathbf{u}\|_{[H^1(\Omega)]^2}^2 + \|\boldsymbol{\xi}_{\tilde{h}} - \boldsymbol{\xi}\|_{[H_{00}^{1/2}(\Gamma_N)]^2}^2 \right).$$

Then, the proof follows taking into account (8) and proceeding with the remaining terms as in [1].  $\square$

#### 4. Numerical experiments

In this section we present some numerical results that illustrate the performance of the augmented mixed finite element scheme (3) for the finite element subspaces defined in Section 2 and of the adaptive algorithms based on the a posteriori error estimates  $\hat{\eta}$  and  $\bar{\eta}$  derived in Section 3.

We recall that, given the Young modulus  $E$  and the Poisson ratio  $\nu$  of a linear elastic material, the corresponding Lamé constants can be computed by  $\mu := \frac{E}{2(1+\nu)}$  and  $\lambda := \frac{E\nu}{(1+\nu)(1-2\nu)}$ . In the examples below, we take  $E = 1$  and consider the values  $\nu = 0.4900$  and  $\nu = 0.4999$ , which yield the following values of  $\mu$  and  $\lambda$ :

$\nu$	$\mu$	$\lambda$
0.4900	0.3356	16.4430
0.4999	0.3334	1666.4444

Given an error indicator  $\zeta := \left( \sum_{T \in \mathcal{T}_h} \zeta_T^2 \right)^{1/2}$ , we consider the following adaptive algorithm:

- (1) Start with a coarse mesh  $\mathcal{T}_h$ .
- (2) Solve the Galerkin scheme for the current mesh  $\mathcal{T}_h$ .
- (3) Compute  $\zeta_T$  for each triangle  $T \in \mathcal{T}_h$ .

- (4) Consider stopping criterion and decide to finish or go to the next step.  
 (5) Use *bisection procedure* to refine each element  $T' \in \mathcal{T}_h$  such that

$$\zeta_{T'} \geq \frac{1}{2} \max\{\zeta_T : T \in \mathcal{T}_h\}.$$

- (6) Define the resulting mesh as the new  $\mathcal{T}_h$  and go to step 2.

Let  $(\boldsymbol{\sigma}, \mathbf{u}, \boldsymbol{\gamma}, \boldsymbol{\xi})$  and  $(\boldsymbol{\sigma}_h, \mathbf{u}_h, \boldsymbol{\gamma}_h, \boldsymbol{\xi}_h)$  be the unique solutions to problems (2) and (3), respectively. We define the individual errors  $e(\boldsymbol{\sigma}) := \|\boldsymbol{\sigma} - \boldsymbol{\sigma}_h\|_{H(\operatorname{div}; \Omega)}$ ,  $e(\mathbf{u}) := \|\mathbf{u} - \mathbf{u}_h\|_{[H^1(\Omega)]^2}$ ,  $e(\boldsymbol{\gamma}) := \|\boldsymbol{\gamma} - \boldsymbol{\gamma}_h\|_{[L^2(\Omega)]^{2 \times 2}}$  and  $e(\boldsymbol{\xi}) := \|\boldsymbol{\xi} - \boldsymbol{\xi}_h\|_{[H_0^1(\Gamma_N)]^2}$ , and the total error

$$e_{\text{total}} := (e(\boldsymbol{\sigma})^2 + e(\mathbf{u})^2 + e(\boldsymbol{\gamma})^2 + e(\boldsymbol{\xi})^2)^{1/2}.$$

The effectivity index of a given a posteriori error estimate  $\zeta$  is then given by  $I(\zeta) := e_{\text{total}}/\zeta$ . Besides, we define the experimental convergence rate as

$$r(e) := -2 \frac{\log(e_{\text{total}}/e'_{\text{total}})}{\log(\mathcal{N}/\mathcal{N}')} ,$$

where  $\mathcal{N}$  and  $\mathcal{N}'$  denote the degrees of freedom (dof) of two consecutive triangulations, and  $e_{\text{total}}$  and  $e'_{\text{total}}$  are the corresponding total errors.

In the table below, we specify the examples to be considered here. We choose the data  $\mathbf{f}$  and  $\mathbf{g}$  so that the exact solution is  $\mathbf{u}(x_1, x_2)$ . The numerical experiments showed in this section were carried out in a notebook *Intel Core i7-820* with four dual processors using a Matlab code.

EXAMPLE	$\Omega$	$\mathbf{u}(x_1, x_2)$
1	$]0, 1[^2$	$u_1(x_1, x_2) = u_2(x_1, x_2) = x_1 x_2 e^{x_1+x_2}$
2	$] - 1, 1[^2 \setminus [0, 1]^2$	$u_1(x_1, x_2) = u_2(x_1, x_2) = r^{5/3} \sin((2\theta - \pi)/3)$
3	$]0, 2[^2 \setminus B[0, 1]$	$\mathbf{u}(x_1, x_2) = 5(1 - x_1^2 - x_2^2)e^{-5(1-x_1^2-x_2^2)^2}(x_1, -x_2)^t$

In order to emphasize the robustness of the a posteriori error estimates  $\hat{\eta}$  and  $\bar{\eta}$  with respect to the Poisson ratio, we first consider Example 1 with  $\Gamma_D := (\{0\} \times [0, 1]) \cup ([0, 1] \times \{0\})$  and  $\Gamma_N := \Gamma \setminus \bar{\Gamma}_D$ . In Tables I and II we present the dof, the total errors, the convergence rates, the values of the a posteriori error estimates  $\hat{\eta}$  and  $\bar{\eta}$  and the corresponding effectivity indices obtained in a sequence of uniform meshes with  $\nu = 0.4900$  and  $\nu = 0.4999$ , respectively, taking  $\kappa_1 = \mu$ ,  $\kappa_2 = \frac{1}{2\mu}$  and  $\kappa_3 = \frac{\mu}{8}$ . We remark that, independently of how large the errors could become, the effectivity indices obtained with the two values of  $\nu$  are very similar (they remain in a neighborhood of 0.9). These results numerically confirm the robustness of  $\hat{\eta}$  and  $\bar{\eta}$  with respect to the Poisson ratio (and hence, with respect to the Lamé parameter  $\lambda$ ).

On the other hand, the feasible values of the stabilization parameter  $\kappa_3$  depend on the unknown constant  $k_D$  from Korn's first inequality. With the aim of studying the robustness of the scheme (3) with respect to the parameter  $\kappa_3$ , we fixed  $\nu = 0.4900$ ,  $\kappa_1 = \mu$  and  $\kappa_2 = \frac{1}{2\mu}$ , and run the code for different values of  $\kappa_3$ . In Tables I, III, IV and V, we display the dof, the total errors, the convergence rates, the values of the a posteriori error estimates and the corresponding effectivity indices for a sequence of uniform meshes using different values of  $\kappa_3$ . We remark that the optimal order of convergence for the total error is achieved in all cases, confirming the robustness of the discrete scheme (3) with respect to the parameter  $\kappa_3$ . Moreover, the effectivity indices are in all cases in a neighborhood of 0.9.

In what follows, we fix  $\nu = 0.4900$ ,  $\kappa_1 = \mu$ ,  $\kappa_2 = \frac{1}{2\mu}$  and  $\kappa_3 = \frac{\mu}{8}$ , and consider Examples 2 and 3 to illustrate the performance of the adaptive algorithms based

TABLE 1. Ex. 1 ( $\nu = 0.4900$ ): Dof, total errors, convergence rates, a posteriori error estimates and effectivity indices (uniform refinement).

$\mathcal{N}$	$e_{\text{total}}$	$r(e_{\text{total}})$	$\hat{\eta}$	$e_{\text{total}}/\hat{\eta}$	$\bar{\eta}$	$e_{\text{total}}/\bar{\eta}$
50	0.9543E+2	—	0.1243E+3	0.7677	0.1261E+3	0.7568
182	0.6781E+2	0.5288	0.7457E+2	0.9094	0.7922E+2	0.8560
686	0.3284E+2	1.0932	0.3553E+2	0.9243	0.3686E+2	0.8909
2654	0.1611E+2	1.0530	0.1720E+2	0.9364	0.1749E+2	0.9206
10430	0.8003E+1	1.0220	0.8472E+1	0.9447	0.8541E+1	0.9370
41342	0.3995E+1	1.0092	0.4208E+1	0.9494	0.4225E+1	0.9455
164606	0.1996E+1	1.0041	0.2097E+1	0.9519	0.2102E+1	0.9499
656894	0.9980E+0	1.0019	0.1047E+1	0.9532	0.1048E+1	0.9522

TABLE 2. Ex. 1 ( $\nu = 0.4999$ ): Dof, total errors, convergence rates, a posteriori error estimates and effectivity indices (uniform refinement).

$\mathcal{N}$	$e_{\text{total}}$	$r(e_{\text{total}})$	$\hat{\eta}$	$e_{\text{total}}/\hat{\eta}$	$\bar{\eta}$	$e_{\text{total}}/\bar{\eta}$
50	0.9383E+4	—	0.1222E+5	0.7676	0.1240E+5	0.7568
182	0.6688E+4	0.5243	0.7330E+4	0.9123	0.7783E+4	0.8593
686	0.3243E+4	1.0911	0.3490E+4	0.9290	0.3621E+4	0.8954
2654	0.1591E+4	1.0529	0.1688E+4	0.9423	0.1717E+4	0.9264
10430	0.7904E+3	1.0220	0.8310E+3	0.9511	0.8377E+3	0.9435
41342	0.3945E+3	1.0092	0.4126E+3	0.9562	0.4142E+3	0.9523
164606	0.1971E+3	1.0041	0.2056E+3	0.9589	0.2060E+3	0.9569
656894	0.9855E+2	1.0019	0.1026E+3	0.9603	0.1027E+3	0.9593

TABLE 3. Ex. 1 ( $\kappa_3 = \mu/2$ ): Dof, total errors, convergence rates, a posteriori error estimates and effectivity indices (uniform refinement).

$\mathcal{N}$	$e_{\text{total}}$	$r(e_{\text{total}})$	$\hat{\eta}$	$e_{\text{total}}/\hat{\eta}$	$\bar{\eta}$	$e_{\text{total}}/\bar{\eta}$
50	0.9530E+2	—	0.1244E+3	0.7659	0.1261E+3	0.7557
182	0.6773E+2	0.5286	0.7419E+2	0.9129	0.7910E+2	0.8563
686	0.3257E+2	1.1037	0.3525E+2	0.9239	0.3652E+2	0.8918
2654	0.1597E+2	1.0533	0.1713E+2	0.9321	0.1743E+2	0.9160
10430	0.7931E+1	1.0228	0.8452E+1	0.9384	0.8528E+1	0.9300
41342	0.3957E+1	1.0097	0.4199E+1	0.9423	0.4219E+1	0.9378
164606	0.1977E+1	1.0043	0.2093E+1	0.9445	0.2099E+1	0.9422
656894	0.9884E+0	1.0020	0.1045E+1	0.9457	0.1046E+1	0.9445

on the a posteriori error estimates  $\hat{\eta}$  and  $\bar{\eta}$ . In Example 2, we take  $\Gamma_D := (\{0\} \times [0, 1]) \cup ([0, 1] \times \{0\})$ . In this example, the solution has a singularity at the boundary point  $(0, 0)$ . In fact, the behavior of  $\mathbf{u}$  in a neighborhood of the origin implies that  $\mathbf{div}(\boldsymbol{\sigma}) \in [H^{2/3}(\Omega)]^2$  which, according to Theorem 2, yields  $2/3$  as the expected convergence rate for the uniform refinement.

In Tables VI through VIII we provide the dof, the individual and total errors, the experimental convergence rates, the values of the a posteriori error estimates and the corresponding effectivity indices for the uniform and adaptive refinements as

TABLE 4. Ex. 1 ( $\kappa_3 = \mu/16$ ): Dof, total errors, convergence rates, a posteriori error estimates and effectivity indices (uniform refinement).

$\mathcal{N}$	$e_{\text{total}}$	$r(e_{\text{total}})$	$\hat{\eta}$	$e_{\text{total}}/\hat{\eta}$	$\bar{\eta}$	$e_{\text{total}}/\bar{\eta}$
50	0.9546E+2	—	0.1243E+3	0.7681	0.1261E+3	0.7570
182	0.6828E+2	0.5186	0.7491E+2	0.9116	0.7965E+2	0.8573
686	0.3319E+2	1.0874	0.3579E+2	0.9275	0.3727E+2	0.8905
2654	0.1621E+2	1.0595	0.1727E+2	0.9387	0.1760E+2	0.9207
10430	0.8031E+1	1.0262	0.8485E+1	0.9465	0.8559E+1	0.9383
41342	0.4005E+1	1.0103	0.4211E+1	0.9512	0.4229E+1	0.9472
164606	0.2001E+1	1.0044	0.2098E+1	0.9537	0.2103E+1	0.9517
656894	0.1000E+1	1.0020	0.1048E+1	0.9550	0.1049E+1	0.9540

TABLE 5. Ex. 1 ( $\kappa_3 = \mu/32$ ): Dof, total errors, convergence rates, a posteriori error estimates and effectivity indices (uniform refinement).

$\mathcal{N}$	$e_{\text{total}}$	$r(e_{\text{total}})$	$\hat{\eta}$	$e_{\text{total}}/\hat{\eta}$	$\bar{\eta}$	$e_{\text{total}}/\bar{\eta}$
50	0.9547E+2	—	0.1243E+3	0.7683	0.1261E+3	0.7571
182	0.6872E+2	0.5089	0.7536E+2	0.9120	0.8016E+2	0.8573
686	0.3353E+2	1.0819	0.3609E+2	0.9290	0.3771E+2	0.8891
2654	0.1632E+2	1.0640	0.1736E+2	0.9401	0.1776E+2	0.9190
10430	0.8056E+1	1.0320	0.8501E+1	0.9476	0.8585E+1	0.9384
41342	0.4012E+1	1.0122	0.4214E+1	0.9521	0.4233E+1	0.9479
164606	0.2004E+1	1.0049	0.2099E+1	0.9547	0.2104E+1	0.9526
656894	0.1002E+1	1.0021	0.1048E+1	0.9560	0.1049E+1	0.9550

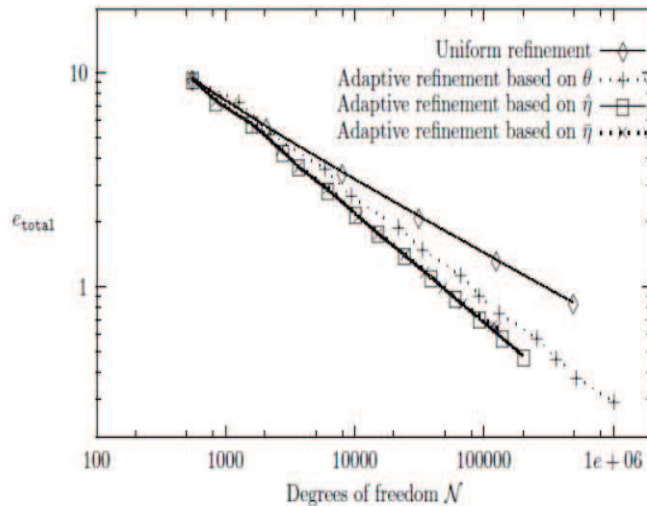


FIGURE 1. Total error vs. dof for the uniform and adaptive refinements (Example 2).

applied to Example 2. We observe from these tables that the errors for the adaptive procedures decrease much faster than for the uniform one, which is confirmed by the

experimental convergence rates. This fact can also be observed in Figure 1, where we display the total error versus the dof for the uniform and adaptive refinements based on  $\theta$ ,  $\hat{\eta}$  and  $\bar{\eta}$ , where  $\theta$  is the a posteriori error estimator proposed in [2].

TABLE 6. Ex. 2: Dof, individual and total errors, experimental convergence rates, a posteriori error estimates and effectivity indices (uniform refinement).

$\mathcal{N}$	$e(\boldsymbol{\sigma})$	$e(\mathbf{u})$	$e(\boldsymbol{\gamma})$	$e(\boldsymbol{\xi})$	$e_{\text{total}}$
550	0.8720E+1	0.1601E+1	0.2928E+1	0.6892E+0	0.9362E+1
2062	0.5441E+1	0.7396E+0	0.1118E+1	0.2458E+0	0.5609E+1
7966	0.3405E+1	0.3408E+0	0.4245E+0	0.9450E-1	0.3449E+1
31294	0.2136E+1	0.1595E+0	0.1718E+0	0.3975E-1	0.2149E+1
124030	0.1342E+1	0.7640E-1	0.7541E-1	0.1673E-1	0.1346E+1
493822	0.8437E+0	0.3732E-1	0.3528E-1	0.6829E-2	0.8452E+0
$\mathcal{N}$	$r(e_{\text{total}})$	$\hat{\eta}$	$e_{\text{total}}/\hat{\eta}$	$\bar{\eta}$	$e_{\text{total}}/\bar{\eta}$
550	—	0.1012E+2	0.9247	0.1021E+2	0.9169
2062	0.7753	0.5843E+1	0.9600	0.5872E+1	0.9553
7966	0.7194	0.3523E+1	0.9790	0.3532E+1	0.9766
31294	0.6918	0.2174E+1	0.9882	0.2177E+1	0.9870
124030	0.6794	0.1356E+1	0.9930	0.1356E+1	0.9924
493822	0.6735	0.8489E+0	0.9956	0.8491E+0	0.9954

In particular, the experimental convergence rates approach  $2/3$  for the uniform refinement procedure (see Table VI) whereas the adaptive procedures based on  $\hat{\eta}$  and  $\bar{\eta}$  are able to recover the rate of convergence  $\mathcal{O}(h)$  for the total error (see Tables VII and VIII). On the other hand, we remark that the effectivity indices in the adaptive procedures remain bounded around the values  $0.8 - 0.9$ , which confirms the reliability and eventual efficiency of  $\hat{\eta}$  and  $\bar{\eta}$ . In Figure 2, we display the effectivity index versus the dof for the adaptive refinements based on  $\theta$ ,  $\hat{\eta}$  and  $\bar{\eta}$ . We observe there that the effectivity indices of  $\hat{\eta}$  and  $\bar{\eta}$  are closer to one than those of  $\theta$ .

TABLE 7. Ex. 2. Adaptive algorithm based on  $\hat{\eta}$ : Dof, individual and total errors, experimental convergence rates, a posteriori error estimates and effectivity indices.

$\mathcal{N}$	$e(\boldsymbol{\sigma})$	$e(\mathbf{u})$	$e(\boldsymbol{\gamma})$	$e(\boldsymbol{\xi})$	$e_{\text{total}}$	$r(e_{\text{total}})$	$\hat{\eta}$	$e_{\text{total}}/\hat{\eta}$
550	0.8720E+1	0.1601E+1	0.2928E+1	0.6892E+0	0.9362E+1	—	0.1012E+2	0.9247
840	0.6935E+1	0.1445E+1	0.2060E+1	0.6962E+0	0.7410E+1	1.1042	0.7987E+1	0.9278
1598	0.5231E+1	0.1221E+1	0.2000E+1	0.7207E+0	0.5777E+1	0.7742	0.6287E+1	0.9189
2780	0.4066E+1	0.7077E+0	0.1142E+1	0.3989E+0	0.4301E+1	1.0660	0.4555E+1	0.9442
3648	0.3432E+1	0.6965E+0	0.1044E+1	0.3017E+0	0.3666E+1	1.1745	0.3903E+1	0.9393
6194	0.2656E+1	0.6006E+0	0.8164E+0	0.2034E+0	0.2850E+1	0.9516	0.3047E+1	0.9353
10049	0.2074E+1	0.3823E+0	0.6256E+0	0.1354E+0	0.2204E+1	1.0623	0.2354E+1	0.9362
15047	0.1685E+1	0.3005E+0	0.4863E+0	0.9917E-1	0.1782E+1	1.0517	0.1896E+1	0.9402
24239	0.1334E+1	0.2612E+0	0.3654E+0	0.9098E-1	0.1411E+1	0.9812	0.1500E+1	0.9404
38599	0.1051E+1	0.1806E+0	0.3108E+0	0.4806E-1	0.1112E+1	1.0239	0.1188E+1	0.9358
59993	0.8405E+0	0.1402E+0	0.2279E+0	0.3713E-1	0.8829E+0	1.0453	0.9370E+0	0.9423
92419	0.6775E+0	0.1222E+0	0.1848E+0	0.3699E-1	0.7137E+0	0.9843	0.7584E+0	0.9411
139024	0.5488E+0	0.9463E-1	0.1505E+0	0.2516E-1	0.5774E+0	1.0384	0.6141E+0	0.9402
202849	0.4564E+0	0.7395E-1	0.1183E+0	0.1638E-1	0.4776E+0	1.0049	0.5057E+0	0.9443

Finally, in Figures 3 and 4, we display some intermediate meshes obtained for Example 2 with the adaptive algorithms based on  $\hat{\eta}$  and  $\bar{\eta}$ , respectively. We remark that both algorithms are able to localize the singularity of the solution at  $(0, 0)$  since the adapted meshes are highly refined around the origin.

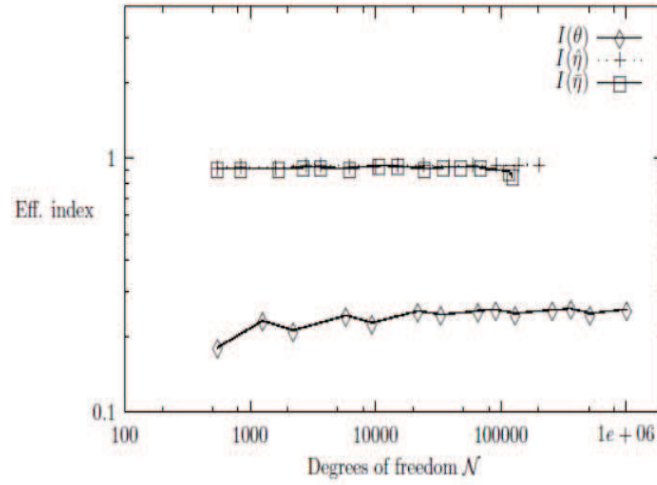


FIGURE 2. Effectivity indices vs. dof for adaptive refinements (Example 2)

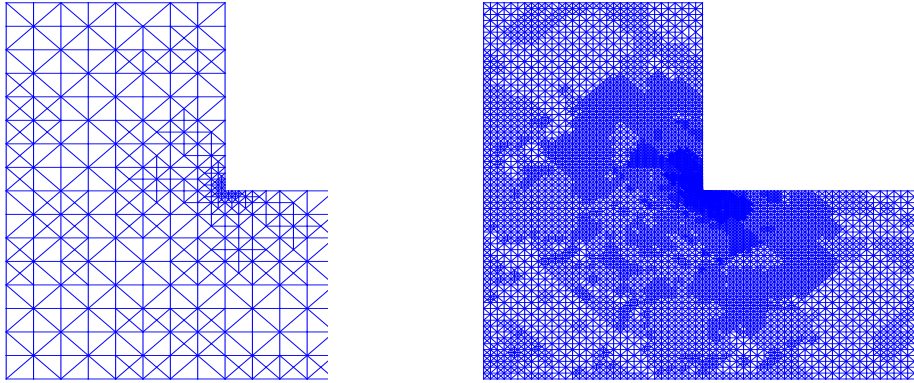


FIGURE 3. Adapted meshes obtained using  $\hat{\eta}$  in Example 2 with 2648 dof (left) and 62410 dof (right)

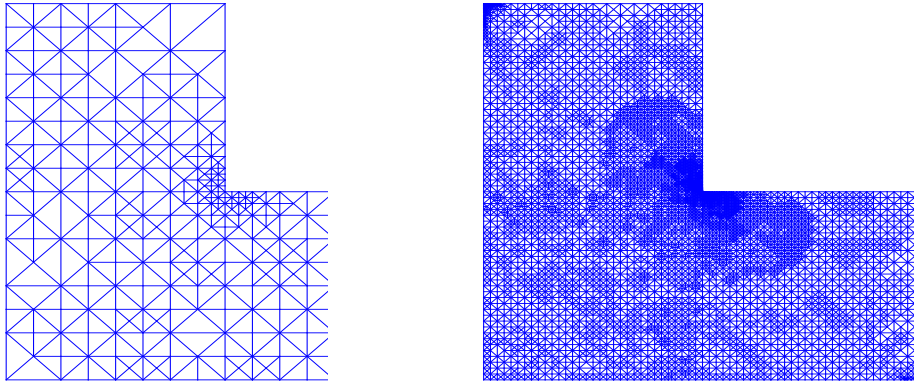


FIGURE 4. Adapted meshes obtained using  $\bar{\eta}$  in Example 2 with 2657 dof (left) and 69092 dof (right).

TABLE 8. Ex. 2. Adaptive algorithm based on  $\bar{\eta}$ : Dof, individual and total errors, experimental convergence rates, a posteriori error estimates and effectivity indices.

$\mathcal{N}$	$e(\boldsymbol{\sigma})$	$e(\mathbf{u})$	$e(\boldsymbol{\gamma})$	$e(\boldsymbol{\xi})$	$e_{\text{total}}$	$r(e_{\text{total}})$	$\bar{\eta}$	$e_{\text{total}}/\bar{\eta}$
550	0.8720E+1	0.1601E+1	0.2928E+1	0.6892E+0	0.9362E+1	—	0.1021E+2	0.9169
840	0.6935E+1	0.1445E+1	0.2060E+1	0.6962E+0	0.7410E+1	1.1042	0.8094E+1	0.9155
1700	0.5156E+1	0.1268E+1	0.1857E+1	0.6590E+0	0.5664E+1	0.7626	0.6193E+1	0.9145
2657	0.4112E+1	0.7808E+0	0.1196E+1	0.3527E+0	0.4367E+1	1.1641	0.4707E+1	0.9278
3648	0.3434E+1	0.6903E+0	0.1017E+1	0.3125E+0	0.3661E+1	1.1129	0.3945E+1	0.9279
6195	0.2669E+1	0.5728E+0	0.9052E+0	0.3309E+0	0.2895E+1	0.8868	0.3175E+1	0.9119
10666	0.2045E+1	0.3393E+0	0.5667E+0	0.1133E+0	0.2152E+1	1.0910	0.2303E+1	0.9348
15118	0.1689E+1	0.2989E+0	0.4868E+0	0.1022E+0	0.1786E+1	1.0705	0.1919E+1	0.9305
24628	0.1331E+1	0.2564E+0	0.4095E+0	0.8451E-1	0.1419E+1	0.9423	0.1545E+1	0.9182
34889	0.1114E+1	0.1933E+0	0.3416E+0	0.5347E-1	0.1182E+1	1.0480	0.1282E+1	0.9222
48280	0.9491E+0	0.1590E+0	0.2620E+0	0.4081E-1	0.9982E+0	1.0415	0.1077E+1	0.9266
69092	0.8021E+0	0.1327E+0	0.2214E+0	0.3359E-1	0.8433E+0	0.9409	0.9148E+0	0.9219
116723	0.6210E+0	0.1073E+0	0.1850E+0	0.2809E-1	0.6574E+0	0.9498	0.7408E+0	0.8874
124903	0.6124E+0	0.1040E+0	0.1780E+0	0.2707E-1	0.6468E+0	0.4830	0.7580E+0	0.8532

In Example 3, we take  $\Gamma_D := \{\mathbf{x} := (x_1, x_2)^t \in \mathbb{R}^2 : x_1^2 + x_2^2 = 1\}$ . In this case, the solution shows large stress regions in a neighborhood of the Dirichlet boundary  $\Gamma_D$ . In Tables IX through XI we provide the dof, the individual and total errors, the experimental convergence rates, the values of the a posteriori error estimates and the corresponding effectivity indices for the uniform and adaptive refinements as applied to Example 3. We notice from these Tables that the adaptive algorithms converge faster than the uniform refinement procedure. This fact can also be observed from Figure 5 below. On the other hand, we also remark that the effectivity indices are in all cases in a neighborhood of 0.99, which confirms the reliability and eventual efficiency of  $\hat{\eta}$  and  $\bar{\eta}$ . In Figure 6, we display the effectivity index versus the dof for the adaptive refinements based on  $\theta$ ,  $\hat{\eta}$  and  $\bar{\eta}$ .

TABLE 9. Ex. 3: Dof, individual and total errors, experimental convergence rates, a posteriori error estimates and effectivity indices (uniform refinement).

$\mathcal{N}$	$e(\boldsymbol{\sigma})$	$e(\mathbf{u})$	$e(\boldsymbol{\gamma})$	$e(\boldsymbol{\xi})$	$e_{\text{total}}$
1420	0.3345E+3	0.3673E+2	0.2654E+2	0.1895E+2	0.3381E+3
6784	0.1772E+3	0.1325E+2	0.2863E+2	0.8648E+1	0.1802E+3
30583	0.8631E+2	0.4538E+1	0.1098E+2	0.1310E+1	0.8713E+2
130076	0.4261E+2	0.2135E+1	0.4027E+1	0.9800E+0	0.4287E+2
541627	0.2113E+2	0.1520E+1	0.1671E+1	0.1036E+1	0.2127E+2
$\mathcal{N}$	$r(e_{\text{total}})$	$\hat{\eta}$	$e_{\text{total}}/\hat{\eta}$	$\bar{\eta}$	$e_{\text{total}}/\bar{\eta}$
1420	—	0.3388E+3	0.9979	0.3390E+3	0.9972
6784	0.8044	0.1824E+3	0.9880	0.1826E+3	0.9868
30583	0.9653	0.8790E+2	0.9913	0.8795E+2	0.9908
130076	0.9800	0.4306E+2	0.9954	0.4308E+2	0.9951
541627	0.9823	0.2126E+2	1.0008	0.2126E+2	1.0006

Finally, in Figures 7 and 8 we display some intermediate meshes obtained for Example 3 with the adaptive algorithms based on  $\hat{\eta}$  and  $\bar{\eta}$ , respectively. We remark that both algorithms are able to localize the large stress regions of the solution since the adapted meshes concentrate the refinements around the Dirichlet boundary, where the large stresses occur.

TABLE 10. Ex. 3. Adaptive algorithm based on  $\hat{\eta}$ : Dof, individual and total errors, experimental convergence rates, a posteriori error estimates and effectivity indices.

$\mathcal{N}$	$e(\sigma)$	$e(\mathbf{u})$	$e(\gamma)$	$e(\xi)$	$e_{\text{total}}$	$r(e_{\text{total}})$	$\hat{\eta}$	$e_{\text{total}}/\hat{\eta}$
1420	0.3345E+3	0.3673E+2	0.2654E+2	0.1895E+2	0.3381E+3	—	0.3388E+3	0.9979
2185	0.1935E+3	0.1491E+2	0.2871E+2	0.6756E+1	0.1963E+3	2.5231	0.1985E+3	0.9890
3714	0.1223E+3	0.9772E+1	0.1821E+2	0.8330E+1	0.1243E+3	1.7212	0.1255E+3	0.9908
6358	0.9079E+2	0.6692E+1	0.1317E+2	0.2539E+1	0.9201E+2	1.1201	0.9295E+2	0.9900
11903	0.6205E+2	0.4095E+1	0.8144E+1	0.1385E+1	0.6273E+2	1.2220	0.6324E+2	0.9919
22789	0.4488E+2	0.2927E+1	0.5626E+1	0.1022E+1	0.4534E+2	0.9999	0.4567E+2	0.9926
43726	0.3119E+2	0.2150E+1	0.3702E+1	0.8996E+0	0.3150E+2	1.1178	0.3167E+2	0.9946

TABLE 11. Ex. 3. Adaptive algorithm based on  $\bar{\eta}$ : Dof, individual and total errors, experimental convergence rates, a posteriori error estimates and effectivity indices.

$\mathcal{N}$	$e(\sigma)$	$e(\mathbf{u})$	$e(\gamma)$	$e(\xi)$	$e_{\text{total}}$	$r(e_{\text{total}})$	$\bar{\eta}$	$e_{\text{total}}/\bar{\eta}$
1420	0.3345E+3	0.3673E+2	0.2654E+2	0.1895E+2	0.3381E+3	—	0.3390E+3	0.9972
2185	0.1935E+3	0.1491E+2	0.2871E+2	0.6756E+1	0.1963E+3	2.5231	0.1987E+3	0.9876
3714	0.1223E+3	0.9772E+1	0.1821E+2	0.8330E+1	0.1243E+3	1.7212	0.1258E+3	0.9888
6358	0.9079E+2	0.6692E+1	0.1317E+2	0.2539E+1	0.9201E+2	1.1201	0.9316E+2	0.9877
11903	0.6205E+2	0.4095E+1	0.8144E+1	0.1385E+1	0.6273E+2	1.2220	0.6333E+2	0.9905
22855	0.4481E+2	0.2901E+1	0.5598E+1	0.1013E+1	0.4526E+2	1.0004	0.4565E+2	0.9916
43746	0.3119E+2	0.2148E+1	0.3689E+1	0.8970E+0	0.3149E+2	1.1176	0.3168E+2	0.9940

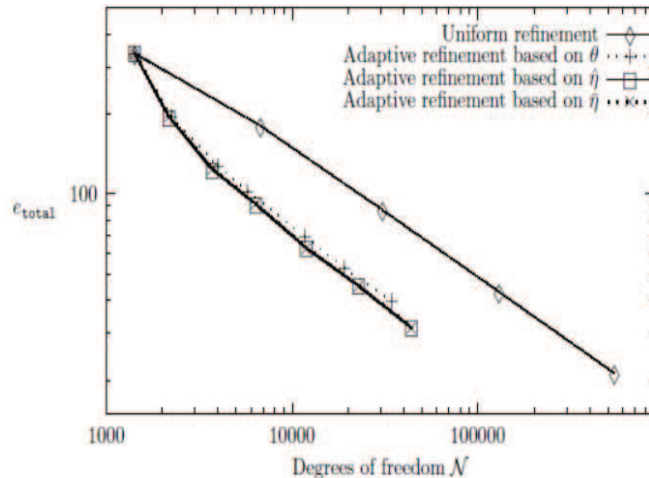


FIGURE 5. Total error vs. dof for the uniform and adaptive refinements (Example 3).

We end this section with some numerical results concerning the performance of the augmented mixed finite element scheme (3) and the adaptive algorithms based on the a posteriori error estimates  $\hat{\eta}$  and  $\bar{\eta}$  to approximate the solution of the classical Cook's membrane problem. We consider the domain  $\Omega := [0, 48] \times [0, 60] \setminus \{(x_1, x_2) \in \mathbb{R}^2 / x_2 < \frac{11x_1}{12} \text{ or } x_2 > \frac{x_1}{3}\}$ ,  $\Gamma_D := \{(x_1, x_2) \in \bar{\Omega} / x_1 = 0\}$  and  $\Gamma_N = \partial\Omega \setminus \bar{\Gamma}_D$ . We assume the data  $\mathbf{f} = \mathbf{0}$  and  $\mathbf{g}(x_1, x_2) = (0, 1)$  if  $(x_1, x_2) \in \Gamma_N$  with  $x_1 = 48$  and  $\mathbf{g} = (0, 0)$  on the remaining part of  $\Gamma_N$ . The material parameters are  $E = 2900$  and  $\nu = 0.3$ . We use the estimates  $\hat{\eta}$  and  $\bar{\eta}$  to show the convergence behavior for the uniform and adaptive refinements (see Figures 9 and 10). We

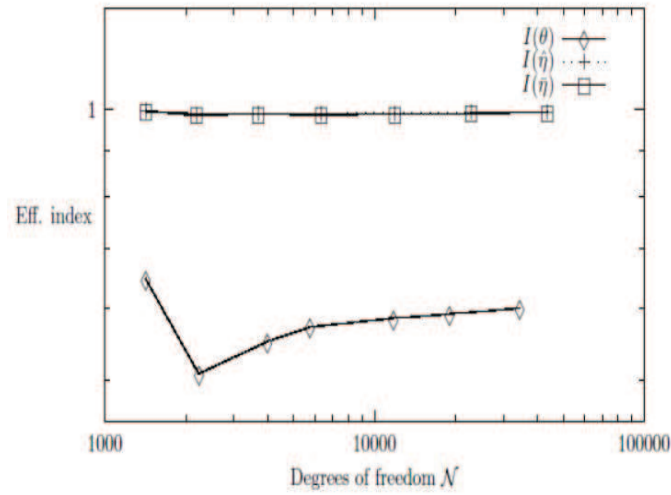


FIGURE 6. Effectivity indices vs. dof for adaptive refinements (Example 3)

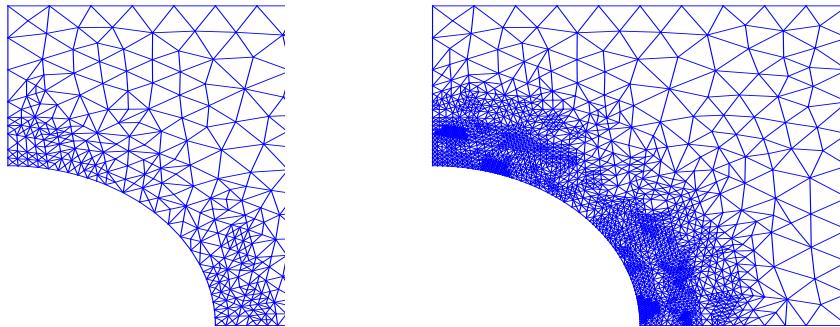


FIGURE 7. Adapted meshes obtained using  $\hat{\eta}$  in Example 3 with 3714 dof (left) and 22789 dof (right)

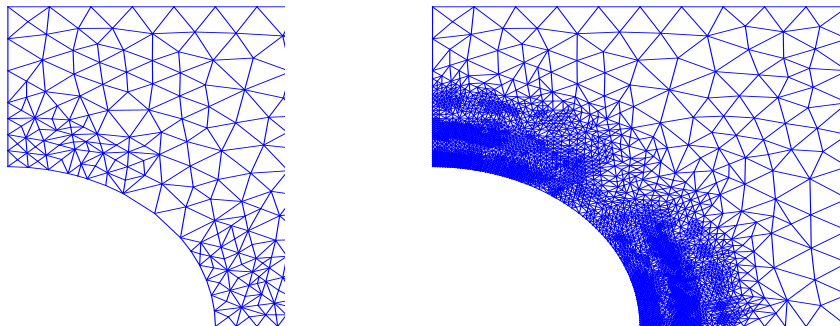


FIGURE 8. Adapted meshes obtained using  $\bar{\eta}$  in Example 3 with 2185 dof (left) and 43746 dof (right).

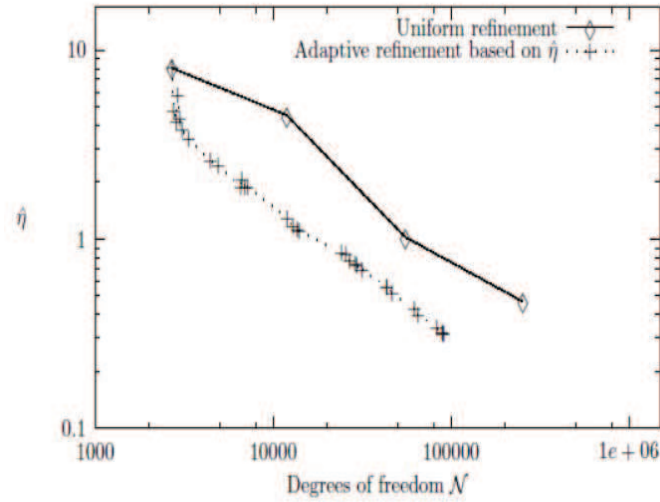


FIGURE 9. Estimator  $\hat{\eta}$  vs. dof for adaptive and uniform refinements (Cook's membrane).

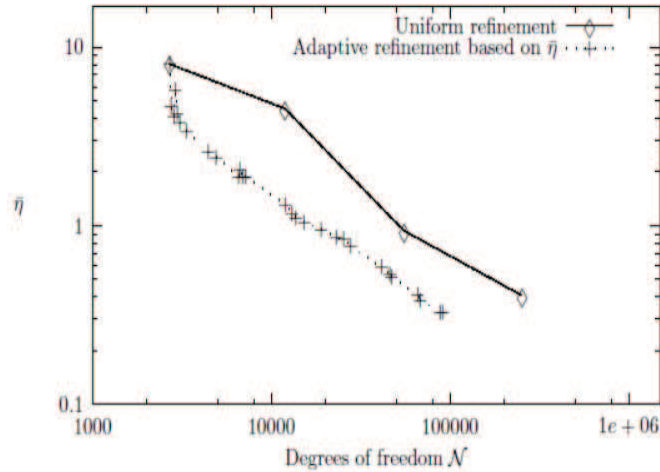


FIGURE 10. Estimator  $\bar{\eta}$  vs. dof for adaptive and uniform refinements (Cook's membrane).

observe from these pictures that the errors of the adaptive procedures decrease much faster than those obtained by the uniform one.

Some intermediate meshes obtained with the adaptive refinements are shown in Figures 11 and 12. We remark that the algorithm is able to recognize the large stress regions of the solution.

In summary, the numerical results provided in this section confirm the reliability of the a posteriori error estimates  $\hat{\eta}$  and  $\bar{\eta}$ , and support their eventual efficiency in practice. The associated adaptive algorithms are able to localize the singularities and large stress regions of the solution. Hence, they become much more suitable

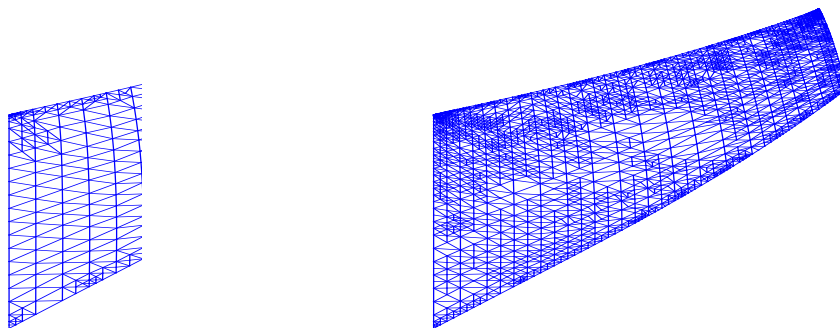


FIGURE 11. Adapted meshes obtained using  $\hat{\eta}$  in Cook's membrane with 4890 dof (left) and 25581 dof (right).

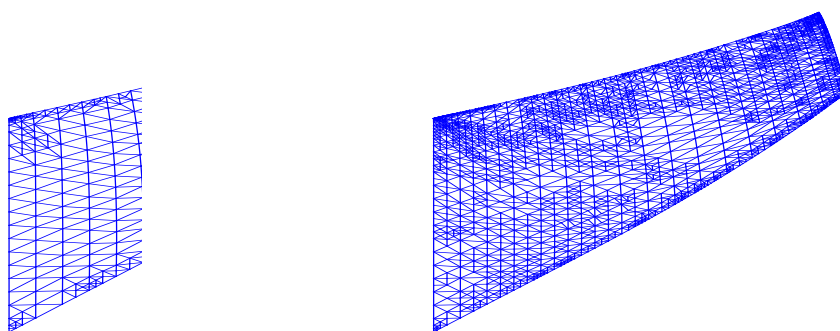


FIGURE 12. Adapted meshes obtained using  $\bar{\eta}$  in Cook's membrane with 4890 dof (left) and 25581 dof (right).

than the corresponding uniform refinement procedure when solving problems with non-smooth solutions.

## 5. Conclusions

We introduced two new a posteriori error estimators for the augmented mixed finite element method proposed in [7] for the linear elasticity problem in the plane with mixed boundary conditions. The first a posteriori error estimator,  $\hat{\eta}$ , is reliable and requires the computation of 4 residuals per element in the interior triangles and in the triangles with a side on the Dirichlet boundary; in the triangles with a side on the Neumann boundary, it requires the computation of 6 residuals per element. The second a posteriori error estimator,  $\bar{\eta}$ , is reliable and locally efficient in the elements that does not touch the Neumann boundary. It requires the computation of 5 residuals per element in interior triangles and triangles with a side on the Dirichlet boundary; in triangles with a side on the Neumann boundary, 7 residuals need to be computed. As compared with the a posteriori error estimator  $\theta$  introduced in [2], which is reliable and efficient, the new a posteriori error estimators are less expensive and easier to implement (the computation of the error indicator  $\theta$  involves 13 terms per triangle, including normal and tangential jumps). From a practical point of view, the performance of the three a posteriori error estimators is very similar. All estimators recognize the singularities and large stress regions of the solutions. Effectivity indices of  $\hat{\eta}$  and  $\bar{\eta}$  are closer to one than those of  $\theta$ . In view of the numerical results, we recommend the use of  $\hat{\eta}$  or  $\bar{\eta}$ .

## Acknowledgments

The first and second authors were partially supported by CONICYT-Chile through FONDECYT grant 1160578, and by Dirección de Investigación of Universidad Católica de la Santísima Concepción (Chile). The research of the third author is partially supported by Spanish Ministerio de Economía y Competitividad grant MTM2016-76497-R.

## References

- [1] Barrios, T.P., Gatica, G.N., González, M. and Heuer, N., A residual based a posteriori error estimator for an augmented mixed finite element method in linear elasticity, *M2AN Math. Model. Numer. Anal.* 40, 843–869 (2006).
- [2] Barrios, T.P., Behrens, E.M. and González, M., A posteriori error analysis of an augmented mixed formulation in linear elasticity with mixed and Dirichlet boundary conditions, *Comput. Methods Appl. Mech. Engrg.* 200, 101–113 (2011).
- [3] Barrios, T.P., Behrens, E.M. and González, M., Low cost a posteriori error estimators for an augmented mixed FEM in linear elasticity, *Appl. Numer. Math.* 84, 46–65 (2014).
- [4] Brezzi, F. and Fortin, M., *Mixed and hybrid finite element methods*, Springer Series in Computational Mathematics 15, Springer-Verlag, New York, 1991.
- [5] Carstensen, C., An a posteriori error estimate for a first-kind integral equation, *Math. Comp.* 66, 139–155 (1997).
- [6] Carstensen, C. and Dolzmann, G., A posteriori error estimates for mixed FEM in elasticity, *Numer. Math.* 81, 187–209 (1998).
- [7] Gatica, G.N., Analysis of a new augmented mixed finite element method for linear elasticity allowing  $\mathcal{RT}_0$ - $\mathcal{P}_1$ - $\mathcal{P}_0$  approximations, *M2AN Math. Model. Numer. Anal.* 40, 1–28 (2006).
- [8] Gatica, G.N., An augmented mixed finite element method for linear elasticity with non-homogeneous Dirichlet conditions, *Electronic Transactions on Numerical Analysis*, vol. 26, pp. 421–438 (2007).
- [9] Gatica, G.N., Márquez, A. and Meddahi, S., An augmented mixed finite element method for 3D linear elasticity problems, *J. Comput. Appl. Math.* 231, 2, 526–540 (2009).
- [10] Gatica, G.N., Oyarzúa, R. and Sayas, F.-J., Analysis of fully-mixed finite element methods for the Stokes-Darcy coupled problem, *Math. Comp.* 80 (276) pp. 1911–1948 (2011).
- [11] González, M., Stabilized dual-mixed method for the problem of linear elasticity with mixed boundary conditions, *Applied Mathematics Letters* 30, pp. 1-5 (2014).

Departamento de Matemática y Física Aplicadas, Universidad Católica de la Santísima Concepción, Concepción, Chile

*E-mail:* tomas@ucsc.cl

Departamento de Ingeniería Civil, Universidad Católica de la Santísima Concepción, Concepción, Chile

*E-mail:* ebehrens@ucsc.cl

Departamento de Matemáticas, Universidade da Coruña, A Coruña, 15071, Spain and Basque Center for Applied Mathematics, Bilbao, 48009, Spain

*E-mail:* maria.gonzalez.taboada@udc.es

*URL:* <http://orcid.org/0000-0002-5576-1582>